IEEE Access
Multidisciplinary | Rapid Review | Open Access Journal

Received September 3, 2021, accepted September 18, 2021, date of publication September 22, 2021,
date of current version October 4, 2021.

Digital Object Identifier 10.1109/ACCESS.2021.3114442

Configuration Detection of Grounding Grid: Static Electric Field Based Nondestructive Technique

AAMIR QAMAR[1], SHAHID IQBAL[1], SADIQ AHMAD[1], (Member, IEEE), ABBAS Z. KOUZANI[2], (Member, IEEE), AND M. A. PARVEZ MAHMUD[2], (Member, IEEE)

[1]Department of Electrical and Computer Engineering, COMSATS University Islamabad, Wah Campus 47040, Pakistan
[2]School of Engineering, Deakin University, Melbourne, VIC 3217, Australia

Corresponding author: Sadiq Ahmad (engrsadiqahmad@ciitwah.edu.pk)

ABSTRACT Grounding grid configuration which, is key to its fault diagnosis, changes continuously with the extension in a substation. Furthermore, older substations grounding grid configurations are unknown. Existing literature regarding configuration detection mainly accounts for the magnetic field that required a gradient to locate the grounding conductor. The gradient of raw measurement in the substation vicinity enhances electromagnetic noise and distorts the results. Therefore, in this paper, we have developed a new algorithm, Configuration Detection of Grounding Grid (CDGG) based on the static electric field and the concept of ordered pairs to draw the configuration of the unknown grounding grid. Unlike, the practiced magnetic field, the electric field does not require a gradient. The maximum electric field value indicates the location of a grounding conductor. The connection between nodes is verified by measuring the electric field on the circle. Furthermore, the proposed algorithm also locates any diagonal conductor in the configuration. Mathematical reasoning and simulation results illustrate that our proposed algorithm is feasible to draw the configuration of the unknown grounding grid.

INDEX TERMS CDGG, grounding grid, static electric field.

I. INTRODUCTION

The grounding grid is a part of a grounding system that provides regular protection to a substation and operators. Grounding grid is responsible to discharge fault currents in the case of a lightning strike, surges, and short circuit to the Earth. This empowers it to keep the step, touch and ground potential restricted [1], [2]. Bare conductors made up of metals or alloys are welded together to build a grounding grid. This includes copper, steel, galvanized steel, etc. Grounding grid is buried 0.3m to 0.5m below the earth's surface and its mesh size can vary from 3m to 7m [3], [4]. The applications of the grounding grid include the protection of underground pipelines against stray currents, computer station, power substations and traction substations, etc. [5], [6].

Grounding grid is prone to faults due to loose connection or the nature of the soil where it is buried. Faults like corrosion and breakage occur in the grounding grid due to the presence of dissolved oxygen in clay as well as the presence of acid in moisture [4], [7]. Therefore, the researchers over time have developed various methods to diagnose grounding grid faults. These methods include the electromagnetic methods [8]–[12], the electrochemical methods [13]–[15] and methods based on network theory [16]–[20]. The electromagnetic methods are further classified as current injection methods [21]–[23] and transient electromagnetic methods (TEM) [8], [10], [11]. However, the current injection electromagnetic methods are usually accompanied by gradient method that enhances the substation electromagnetic noise. Furthermore, the TEM-based fault diagnosis methods claim of being independent of grounding grid layout is false. This is because TEM methods fail to distinguish between missing and broken conductors. In [12], the authors analyze the modern control techniques to determine the most effective ones to monitor the status of grounding of current energy objects in operation. The criteria for analyzing was based on comparing the experimental and calculation techniques for determining the rated parameters of the grounding of existing energy objects.

The electric network methods take the grounding conductor resistance as the fault parameter, adopting the non-linear optimization method, merging the diagnosis with the network theory and comparative analysis with the original data, to diagnose corrosion and breakpoint in the

The associate editor coordinating the review of this manuscript and approving it for publication was Zhouyang Ren.

grounding conductor. Electric network methods are further classified as port resistance, sensitivity analysis and improved sensitivity analysis methods. However, the drawbacks are associated with these methods, i.e. the sensitivity analysis method accounts a very limited number of equations and does not take the non-linearity into consideration which leads the resistance of each conductor segment to diverge greatly from the actual value. Moreover, the authors in [19] proposed the branch voltage disturbance for the corrosion diagnosis. This technique can locate and judge the degree of corrosion through branch voltage disturbance before and after corrosion. Electrochemical methods only focus on the corrosion diagnosis of a grounding grid by measuring the electrochemical characteristics of soil and grounding conductors.

With extension, new equipment is added to a substation that changes the configuration of the grounding grid as well. As the grounding grid configuration is a pre-requisite to its fault diagnosis, therefore, researchers are working to develop methods to draw the configuration of the grounding grid before its fault diagnosis. The literature on configuration detection is quite limited. This includes mainly the electromagnetic methods [3], [23]–[25]. In [3], the authors take the transient electromagnetic method into account to draw the configuration of the grounding grid. Equivalent resistivity is calculated using the inversion calculation from the secondary magnetic field measured at the receiving coil. However, the authors did not consider the diagonal branch. In [23], the magnetic detection electrical impedance (MDEIT) is utilized to determine the resistivity of a grounding grid from the surface magnetic field. The shortcoming of this method is the numerous measurements. Furthermore, [24] used the gradient method and the concept of ordered pairs to determine the configuration of the grounding grid. However, the gradient of raw measurement in substation enhances the surrounding EMI making the results twisted.

This paper proposes a new method based on the static electric field to draw the configuration of the unknown grounding grid. Unlike the practiced magnetic field, the static electric field is not accompanied by the gradient method which, enhances the substation electromagnetic (EM) noise. Secondly, the electric field shielding is simple compared to the magnetic field [26]. The concept of ordered pairs is utilized to draw the connections between node points. Moreover, the connections are verified by measuring the electric field on the circle. The proposed method is also able to detect any diagonal branch in the grid configuration. The proposed method algorithm and flow chart is also provided in Section III to enhance the understanding of the method. Simulations are performed in COMSOL Multiphysics 5.0 using its AC/DC module.

In the end, the contributions of this manuscript are as follows:

- The static electric field is processed from a current-carrying conductor instead of the practiced magnetic field.
- A new algorithm the CDGG is developed based on the static electric field and the concept of ordered pairs.
- Unlike the practiced magnetic field, the static electric field is independent of the gradient method for locating a grounding conductor. Therefore, the substation EMI is not enhanced.
- The proposed method's independence from the gradient method decreases its computation complexity.
- Unlike most of the existing methods for configuration detection, the proposed algorithm can also detect a diagonal branch in a grounding grid.

The rest of the paper is arranged such that Section II provides the mathematical modeling, Section III describes the methodology, Section IV is the method validation and verification through simulations and Section V compares the proposed static electric field with the state-of-the-art magnetic field. Finally, Section VI describes the conclusion and the future directions.

II. STATIC ELECTRIC FIELD FROM A CURRENT CARRYING GROUNDING CONDUCTOR

Grounding grid buried in earth traverses the entire substation area. Drawing the configuration of the unknown grounding grid is an inverse problem. A DC current-carrying conductor of infinite length is illustrated in Fig. 1. This conductor is buried at depth h below the earth's surface and placed along the x-axis. The electric field at point P(x, y, h) is expressed as:

$$\vec{E} = \frac{\rho_L}{2\pi\epsilon\rho}\hat{a_\rho} \tag{1}$$

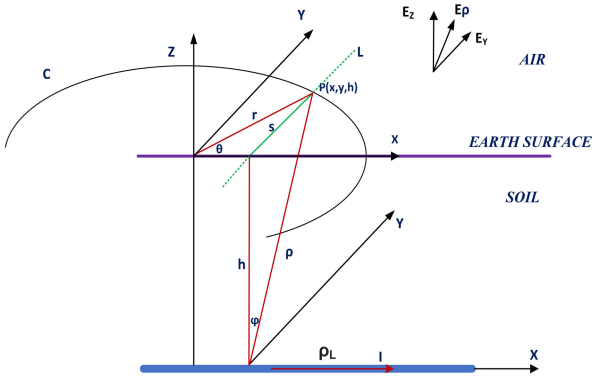

FIGURE 1. A grounding conductor of infinite length is stationed along the x-axis. The conductor is buried in the soil at depth h from the earth's surface and carries a DC current I. ρ_L is the line charge density due to the charges on the surface of the conductor. ρ represents the distance of point $P(x, y, h)$ from the conductor. The C shows the circle of radius r and the L illustrates the line to measure the electric field. The electric field at P(x, y, h) is represented by $\vec{E}_\rho$ where $\vec{E}_Z$ and $\vec{E}_Y$ are its vector components.

The ρ is the distance of the point P from the conductor, ϵ is the permittivity of soil, ρ_L is the line charge density and $\hat{a_\rho}$ is the unit vector showing the direction of the electric field. (1) in rectangular coordinates is expressed as:

$$\vec{E} = \frac{\rho_L}{2\pi\epsilon\rho}\left(\sin\varphi\hat{a_y} + \cos\varphi\hat{a_z}\right) \tag{2}$$

Taking the electric field z-component and expressing it according to Fig. 1:

$$\vec{E}_z = \frac{\rho_L}{2\pi\epsilon\rho}\cos\varphi\hat{a}_z \tag{3}$$

$$\vec{E}_z = \frac{\rho_L}{2\pi\epsilon}\left(\frac{h}{h^2+s^2}\right)\hat{a}_z \tag{4}$$

$$\vec{E}_z = \frac{\rho_L}{2\pi\epsilon}\left(\frac{h}{h^2+r^2\sin^2\theta}\right)\hat{a}_z \tag{5}$$

The θ is the angle with the x-axis when the circle C is traversed. Similarly, (5) can also be expressed as:

$$\vec{E}_z = \frac{\rho_L}{2\pi\epsilon}\left(\frac{h}{h^2+y^2}\right)\hat{a}_z \tag{6}$$

According to (5), the $\vec{E}_z$ is maximum at $\theta = 0$rad and 3.14rad and (6) illustrates that $\vec{E}_z$ is maximum at y = 0m. These outcomes show the location of the buried grounding conductor when the $\vec{E}_z$ is traversed along the circle C and the line L. The simulations of the above discussion are presented in Fig. 2 and Fig. 3. Fig. 2 shows the maximum value of $\vec{E}_z$ at $\theta = 0$rad and 3.14rad and Fig. 3 illustrates the maximum value of $\vec{E}_z$ at y = 0m. These results verify the mathematical reasoning from (1) to (6), which show that the $\vec{E}_z$ from a grounding conductor is maximum at its location.

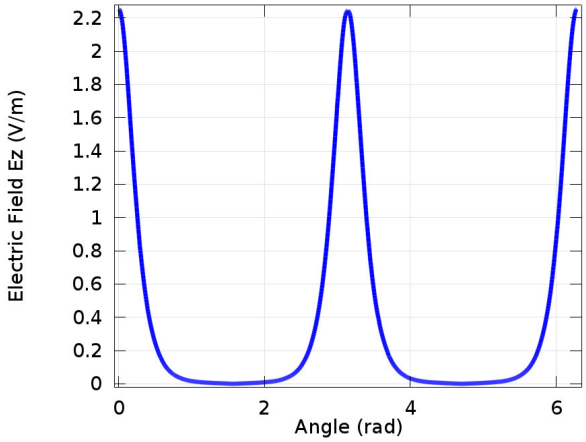

FIGURE 2. Electric field $\vec{E}_z$ along the circle C. The $\vec{E}_z$ is maximum at 0rad and 3.14rad that shows the location of the buried conductor. $\vec{E}_z$ is maximum at two points as the circle traverses the conductor location twice.

The electric field measurement along the line is meant to detect horizontal branches whereas the measurement along the circle serves to detect any angled or diagonal branch in a mesh of a grounding grid. Furthermore, the measurement of the electric field on a circle also serves to verify the existence of a branch between two nodes. This is illustrated in Section IV.

III. GROUNDING GRID CONFIGURATION DETECTION BASED ON STATIC ELECTRIC FIELD

The proposed approach based on the static electric field for configuration detection of the grounding grid follows

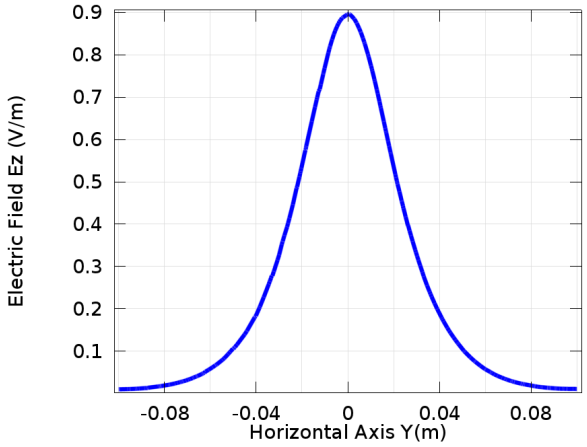

FIGURE 3. Electric field $\vec{E}_z$ along the line L. The $\vec{E}_z$ is maximum at y = 0m that shows the location of the buried conductor as the $\vec{E}_z$ is measured along the line L.

Algorithm 1 The CDGG Algorithm

begin
1) Taking a vertical conductor as the starting point
2) Measure $\vec{E}_{zl}$ on the x and y-axis
3) Plotting N_n from $\left(\vec{E}_{zl} = max\right)$
4) Join all N_n
5) Measure $\vec{E}_{zl}$ $\forall$ lines along the x and y-axis
6) **if** $\left(\vec{E}_{zl} = max\right)$ **then**
   repeat step 3 and 4
   else
   proceed
7) Measure $\vec{E}_{zc}$ $\forall$ N_n
8) **if** $\left(\vec{E}_{zc} = max\right)$ **then**
   g_c $\exists$
   connection retains
   else
   g_c $\nexists$
   remove connection
9) **terminate**

the algorithm, Configuration Detection of Grounding Grid (CDGG) presented in Algorithm 1. Initially, a vertical conductor in the substation is considered as a reference point (origin of the plane). Secondly, the $\vec{E}_{zl}$ which is the electric field on the line is measured along the x and y-axis. The node points N_n are plotted using the concept of ordered pairs from the maximum value of $\vec{E}_{zl}$ against the grounding conductor location and connected to form the mesh. In the fifth and sixth steps, the algorithm measures the $\vec{E}_{zl}$ along the x and y-axis to secure all the node points N_n and connect them to form the complete mesh. The seventh step of the CDGG measures the $\vec{E}_{zc}$ which is the electric field on the circle at each node point to verify the presence of a grounding conductor between two

nodes. The maximum $\vec{E}_{zc}$ at the connection location verifies the grounding conductor while no $\vec{E}_{zc}$ at the connection location does not verify the grounding conductor and the connection in the drawn configuration must be discarded. This step continues until all the connections are verified and the complete configuration of the grid is drawn. Furthermore, the electric field on circle $\vec{E}_{zc}$ also helps to detect diagonal conductor in the grid configuration.

The workflow of the proposed approach is also illustrated in the flowchart in Fig. 4. In the first four steps, the electric field on line $\vec{E}_{zl}$ is measured taking a vertical conductor as the starting point (origin). The maximum value of $\vec{E}_{zl}$ are arranged in ordered pairs, plotted and connected. In the fifth step, the $\vec{E}_{zl}$ is measured on lines along the x and y-axis until all the node points are secured. The sixth step verifies the connection (grounding conductor) between adjacent node points measuring the electric field on the circle which is represented by $\vec{E}_{zc}$. The connection is retained if the $\vec{E}_{zc}$ is maximum at the connection location because the grounding conductor exists otherwise the connection is discarded. This step also detects the presence of any diagonal conductor in the grid configuration.

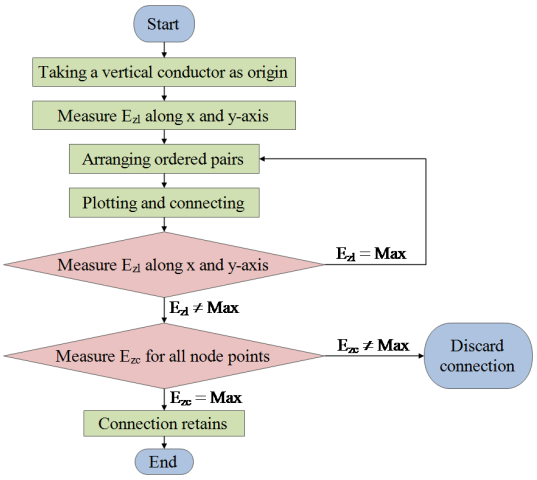

FIGURE 4. Workflow of the static electric field-based configuration detection of grounding grid.

IV. METHOD VALIDATION AND VERIFICATION

To show the effectiveness of the static electric field-based configuration detection of grounding grid, simulations are performed using COMSOL Multiphysics 5.0. COMSOL Multiphysics is a finite element method mathematical modeling software. In this paper, we have solely worked on the AC/DC module of the COMSOL Multiphysics.

A. SIMULATION MODEL

The model to verify the proposed method is shown in Fig. 5 which illustrates a 6m × 6m square grounding grid buried at a depth of 0.2m in a homogeneous soil of permeability μ. The mesh size of the model grid is 3m, the nodes are labeled from 1 to 9 and the branches are labeled from b_1 to b_{12}. The

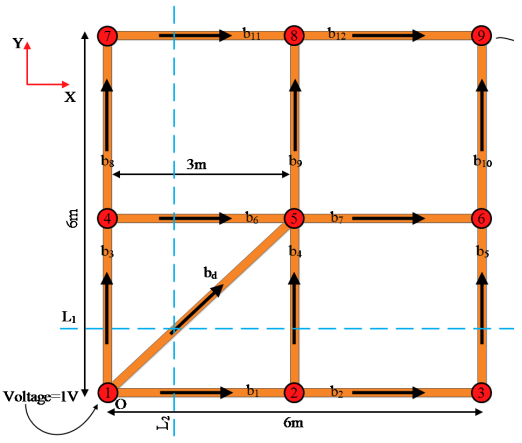

FIGURE 5. The Numerical model illustrated is a 6m × 6m squared mesh grounding grid. The distance between two adjacent branches or mesh size is 3m. The nodes are labeled from 1 to 9 and the branches are represented as b_1 to b_{12}. The b_d shows a diagonal branch connecting node 1 and node 5. DC potential of 1V is applied at a vertical conductor at the origin O and the node 9 is grounded. This drives the current in the grid where the current flow is shown by the arrows. L_1 and L_2 illustrate the lines above the earth's surface for measuring the electric field $\vec{E}_z$.

b_d represents the diagonal branch connecting nodes 1 and 5. In order to apply the proposed algorithm, a DC potential of 1V is applied across the vertical conductor at the origin O (node l) and node 9. The distribution of current in the grid is illustrated by the arrows. Moreover, L_1 and L_2 are the lines along the x and y-axis at the earth's surface to measure the electric field as the second step of the proposed CDGG algorithm.

The proposed CDGG algorithm is applied to the grid model in Fig. 5 such that the vertical conductor at node 1 is considered as the origin O. Following the second step of the CDGG, the electric field $\vec{E}_z$ is measured along the x and y-axis on lines L_1 and L_2. The Fig. 6 and Fig. 7 illustrate the outcome of $\vec{E}_z$ measurement on the line L_1 and L_2. On the line L_1

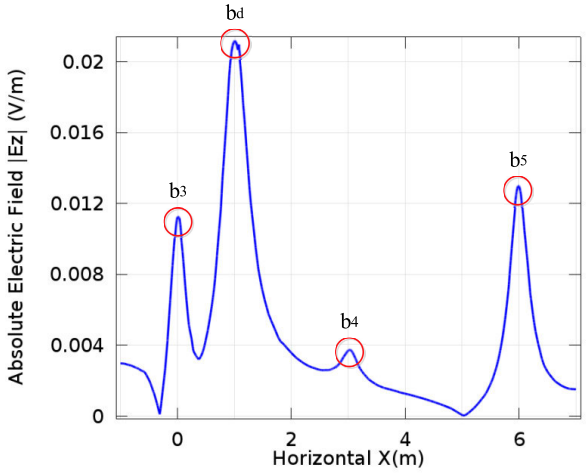

FIGURE 6. The electric field $\vec{E}_z$ on line L_1 along the x-axis. The $\vec{E}_z$ is maximum at 0m, 1m, 3m and 6m representing the branches b_3, b_d, b_4 and b_5 respectively.

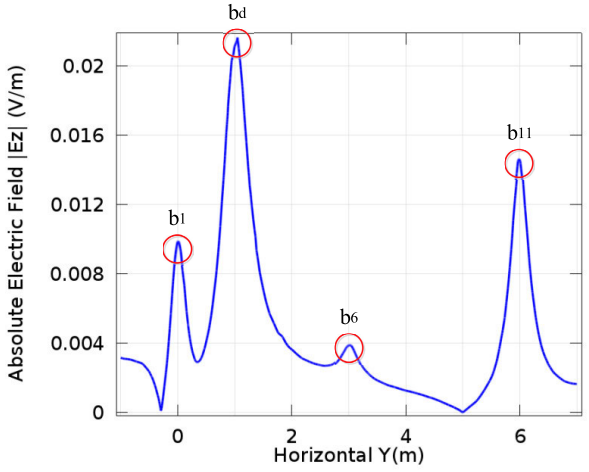

FIGURE 7. The electric field $\vec{E}_z$ on line L_2 along the y-axis. The $\vec{E}_z$ is maximum at 0m, 1m, 3m and 6m representing the branches b_1, b_d, b_6 and b_{11} respectively.

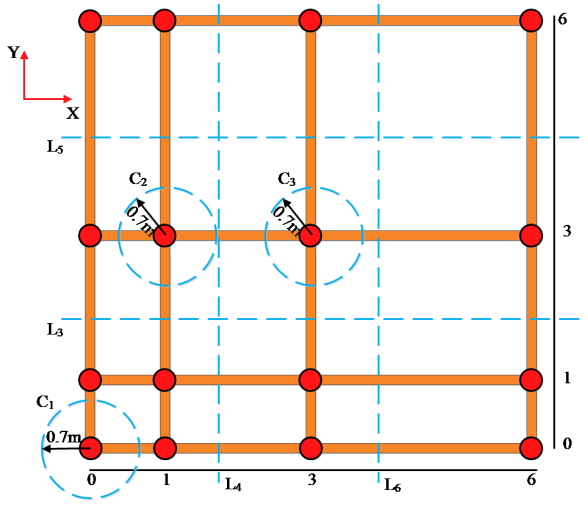

FIGURE 8. The grid configuration is obtained after the fourth step (arranging, plotting and connecting node points) of the CDGG. Line L_3 and L_5 are along the x-axis and line L_4 and L_6 along the y-axis to secure the complete node points. For connection verification, $\vec{E}_z$ is measured along circles centered at each node point. C_1, C_2 and C_3 illustrated are some examples of measuring circles at the earth's surface for the sake of validation.

the maximum $\vec{E}_z$ ($\vec{E}_{zmax}$) is at 0m, 1m, 3m and 6m along the x-axis. Here the $\vec{E}_{zmax}$ at 0m represents the branch b_3, at 1m represents the branch b_d. Although, the location of b_d at 1m along x-axis is wrong, but this is due to the crossover of the line L_1 over the b_d. The correct location of b_d will be diagnosed during the connection verification step of the CDGG. Furthermore, $\vec{E}_{zmax}$ at 3m represents b_4 and at 6m represents b_5. Similarly, the $\vec{E}_z$ is maximum at 0m, 1m, 3m and 6m on line L_2 along the y-axis representing b_1, b_d, b_6 and b_{11}.

The third and fourth step of the algorithm CDGG is the arranging, plotting and connecting the node points obtained by arranging the ordered pairs based on the locations of the $\vec{E}_{zmax}$ along the x and y-axis. The node points obtained are illustrated in Table 1. Plotting and connecting the node points of Table 1, the mesh obtained is shown in Fig. 8. Following the fifth step of the CDGG, $\vec{E}_z$ is measured along the x and y-axis to secure the total number of node points. Therefore, L_3 represents the measuring line along the x-axis on the obtained mesh where the $\vec{E}_z$ is measured. The outcome of the measurement on L_3 is illustrated in Fig. 9. The $\vec{E}_{zmax}$ exists at 0m, 1m, 3m and 6m along the x-axis. This reveals that no new branch is located. Therefore, the third and fourth step of CDGG is skipped as the node points remain the same and the mesh configuration would not alter. Similarly, the measuring line L_4 along the y-axis on the mesh in Fig. 8 would not have

TABLE 1. Ordered pairs based on the location of $\vec{E}_{zmax}$ along L_1 and L_2.

$\vec{E}_{zmax}$ Location along X-axis on L_1	$\vec{E}_{zmax}$ Location along Y-axis on L_2	Node Points
0m	0m	(0,0), (0,1), (0,3), (0,6)
1m	1m	(1,0), (1,1), (1,3), (1,6)
3m	3m	(3,0), (3,1), (3,3), (3,6)
6m	6m	(6,0), (6,1), (6,3), (6,6)

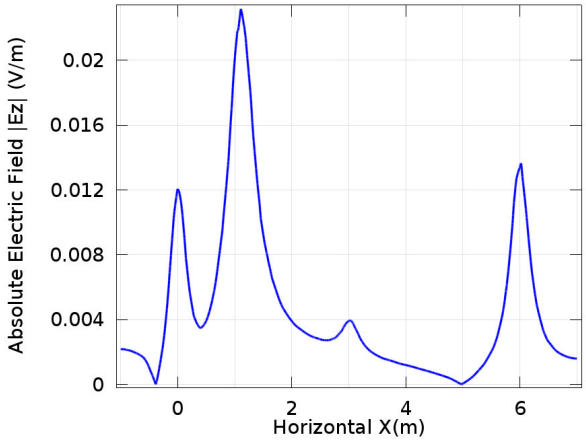

FIGURE 9. The electric field $\vec{E}_z$ on line L_3 along the x-axis. The $\vec{E}_z$ is maximum at 0m, 1m, 3m and 6m.

any impact and the node points would remain unchanged. Measuring $\vec{E}_z$ on line L_5 along the x-axis, the $\vec{E}_{zmax}$ exists at 0m, 3m and 6m illustrated in Fig. 10. Here as well, no new branch is located therefore, the mesh configuration would retain. The same is the case with the outcome of measuring $\vec{E}_z$ on the line L_6 along the y-axis. At the end of the fifth step of the CDGG, the mesh configuration secured is the same as shown in Fig. 8.

In order, to verify the connections between node points, the CDGG takes into account the measurement of $\vec{E}_z$ on a circle at each node point, which is the sixth step of the CDGG. Starting with the node point (0, 0), the $\vec{E}_z$ is measured on the circle C_1 of radius 0.7m at the earth's surface. The radius of the circle depends on the mesh size of the obtained

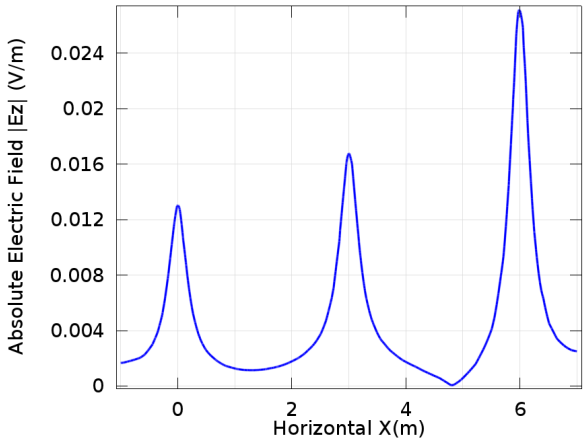

FIGURE 10. The electric field $\vec{E}_z$ on line L_5 along the x-axis. The $\vec{E}_{zmax}$ exists at 0m, 3m and 6m.

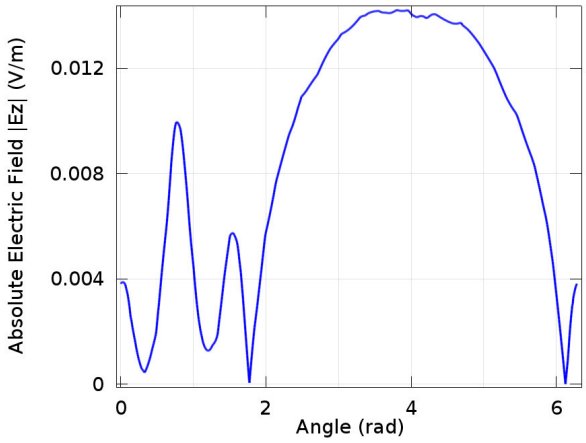

FIGURE 11. The electric field $\vec{E}_z$ on the circle C_1 centered at the node point (0, 0). The $\vec{E}_z$ is maximum at 0rad, 0.785rad and 1.57rad. A new branch is located leading from node point (0, 0) at 45° due to the presence of $\vec{E}_{zmax}$ at 0.785rad.

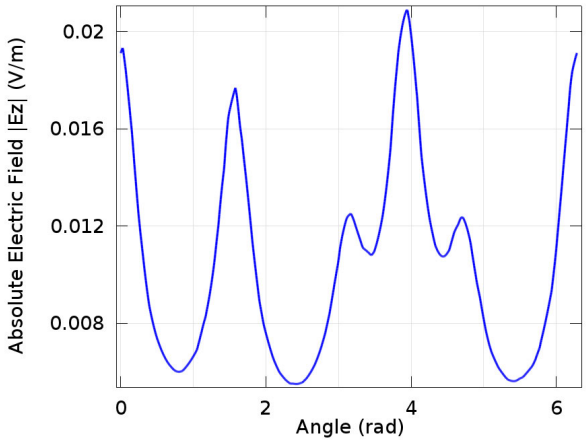

FIGURE 12. The electric field $\vec{E}_z$ on the circle C_3 centered at the node point (3, 3). The $\vec{E}_{zmax}$ is located at 0rad, 1.57rad, 3.14rad, 3.92rad and 4.71 confirming the branch b_7 between node point (3, 3) and (6, 3), the branch b_9 between node point (3, 3) and (3, 6), b_6 between node point (0, 3) and (3, 3), b_d between node point (0, 0) and (3, 3) and b_4 between node point (3, 0) and (3, 3).

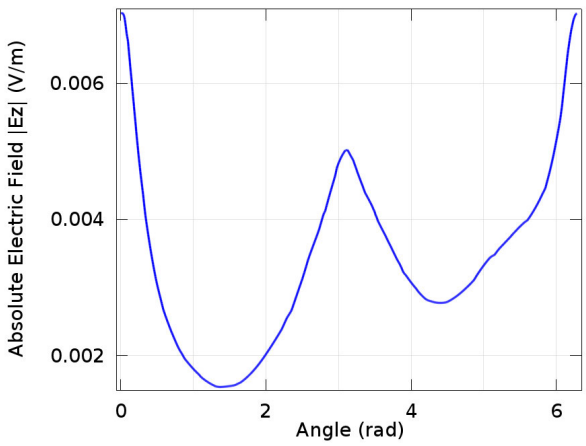

FIGURE 13. The electric field $\vec{E}_z$ on the circle C_2 centered at the node point (1, 3). The $\vec{E}_z$ is maximum at 0rad and 3.14rad confirming the branch b_6 of the simulation model while the branch between the node point (1, 3) and (1, 1) and node point (1, 3) and (1, 6) of the Fig. 8 is discarded as the $\vec{E}_{zmax}$ is not detected at 1.57rad and 4.71rad.

configuration such that the circle should not cross any of the branches that is not connected to the corresponding circle's node point. This is for the sake of locating an object in the polar coordinates. Fig. 11 demonstrates the $\vec{E}_z$ measured on the circle C_1 of radius 0.7m where the $\vec{E}_z$ is maximum at 0rad, 0.785rad and 1.57rad. The $\vec{E}_z$ being maximum at 0rad confirms the branch extending from a node point (0, 0), but to the node point (3, 0). This would be confirmed by measuring $\vec{E}_z$ at node point (1, 0) that would only confirm the existence of a branch between the node point (0, 0) and node point (3, 0). This is the branch that is labeled as b_1 in the simulation model of Fig. 5. Same is the case with $\vec{E}_z$ being maximum at 1.57rad, confirming branch (b_3) between node point (0, 0) and (0, 3) excluding the node point at (1, 0). Moreover, $\vec{E}_{zmax}$ at 0.785rad detects a new branch extending at 45° from the node point (0, 0). This branch that is labeled as diagonal branch d_d in Fig. 5 is further confirmed by measuring $\vec{E}_z$ on the circle at a node point (1, 1) and (3, 3). The outcome of measuring $\vec{E}_z$ at the node point (3, 3) on the circle C_3 is illustrated in Fig. 12. Here the $\vec{E}_z$ is maximum at 0rad, 1.57rad, 3.14rad, 3.92rad and 4.71rad. The $\vec{E}_{zmax}$ at 3.92rad further detects and confirms the b_d between node point (0, 0) and (3, 3). Taking the circle C_2 into account, the $\vec{E}_z$ on it is illustrated in Fig. 13. $\vec{E}_{zmax}$ along the circle C_2 is located at 0rad and 3.14rad which confirms the branch b_4 between node point (0, 3) and (3, 3) while rejects the branch between the node point (1, 1) and (1, 3) and node point (1, 3) and (1, 6). Verifying connections across the whole mesh obtained at the end of the fifth step of CDGG, the mesh configuration obtained is the same as that of the simulation model presented

TABLE 2. A comparative study of the proposed and the existing methods of configuration detection of a grounding grid.

Ref.	Method	Field Type	Grounding Grid Configuration		Computational Complexity	EM Noise	Remarks
			Square Grid	Diagonal Branch			
[22]	Derivative and ICA	Magnetic Field	✓	✓	ICA for EMI Suppression	×	Costly and Time Consuming
[23]	MDEIT	Magnetic Field	✓	×	Conductivity Inverse Calculations	×	Costly and Time Consuming
[25]	Wavelet Edge	Magnetic Field	✓	×	Wavelet Calculations	×	Time Consuming
[3]	TEM	Magnetic Field	✓	×	Equivalent Resistivity Inverse Calculations	×	Time Consuming
[24]	Derivative Method	Magnetic Field	✓	✓	Derivative Calculations	✓	Highly Affected by EMI
Proposed	CDGG	Static Electric Field	✓	✓	No Extra Calculations	×	Cost and Time Effective

in Fig. 5. The simulation results indicate that the CDGG can measure the configuration of any square grounding grid with high accuracy.

V. LOCATING A GROUNDING CONDUCTOR: THE PROPOSED STATIC ELECTRIC FIELD AND STATE OF THE ART MAGNETIC FIELD

The existing literature on the configuration detection and fault diagnosis of a grounding grid mainly accounted for the magnetic field. This includes the wavelet edge method and magnetic detection impedance tomography for configuration detection [23], [25], etc. Similarly, the gradient method for inverse features extraction and transient electromagnetic method for fault diagnosis [8], [22], etc.

To illustrate the effectiveness of the proposed static electric field over the practiced magnetic field, a comparison is performed in this section with regards to locating a grounding conductor. The grounding conductor shown in Fig. 1 is located using the magnetic field of this conductor. This is accomplished using the derivative of the magnetic flux density $\vec{B}_z$. Fig. 14 shows the electric field $\vec{E}_z$ and the derivative of magnetic flux density $\vec{B}_z$ from the grounding conductor model of Fig. 1. The $\vec{E}_z$ and $\vec{B}'_z$ being maximum at 0rad and 3.14rad detects the location of the conductor along the x-axis, but the graph of the magnetic field is a bit distorted compare to the electric field. This is due to the fact that derivatives of numerical data always generate noise. Moreover, this noise is further enhanced in the harsh electromagnetic surrounding of a real substation. Therefore, to overcome the problem of derivative noise associated with the magnetic field and easy shielding of electric field compared to the magnetic field, the electric field is preferred in the proposed method for configuration detection of a grounding grid.

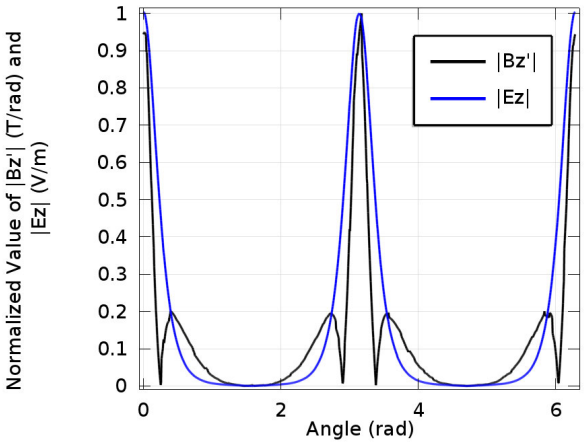

FIGURE 14. Derivative of magnetic flux density $\vec{B}_z$ and the $\vec{E}_z$ on the circle C from the grounding conductor in Fig. 1. The graph of $\vec{B}'_z$ is noisy compare to the graph of $\vec{E}_z$. This is due to the derivative because the derivative of numerical data generates noise.

To establish the superiority of the proposed method over the existing methods a comparative study is illustrated in Table 2. This comparison includes configuration detection, computational complexity and electromagnetic (EM) noise enhancement. The configuration detection is categorized as square grid configuration and square grid configuration including a diagonal branch. Furthermore, the complexity is categorized based on necessary techniques accompanying the main method. For example [22] utilizes the Independent Component Analysis to suppress the electromagnetic interference (EMI) that is enhanced with the derivative method. This comparative study shows that the proposed CDGG algorithm based on static electric field and the concept of ordered pairs are highly effective as compared to the existing configuration detection techniques.

VI. CONCLUSION

A Grounding grid configuration that changes with the extension and development in the substation is key to grounding grid fault diagnosis. In this paper, we have developed a new algorithm, the CDGG based on the static electric field and the concept of ordered pairs to draw the configuration of an unknown grounding grid. The static electric field is proposed compare to the practiced magnetic field due to its independence of the derivative method. The derivative of numerical data generates noise which would even be greater in the strong electromagnetic environment of a real substation. Furthermore, the proposed CDGG algorithm is also able

to locate a diagonal branch in the grid configuration which is a much-needed development with respect to the existing literature on configuration detection of a grounding grid. The mathematical reasoning and simulation results illustrate the viability of the proposed algorithm. Furthermore, a brief comparison between static electric field and magnetic field against locating a grounding conductor is included that shows the effectiveness of electric field over the practiced magnetic field.

As future work, the proposed method would be tested in a real substation. Moreover, the authors would focus on the circular configuration detection of the grounding grid.

REFERENCES

[1] *IEEE Guide for Safety in AC Substation Grounding—Redline*, Standard IEEE Std 80-2013 (Revision of IEEE Std 80-2000/ Incorporates IEEE Std 80-2013/Cor 1-2015) Redline, 2015, pp. 1–426.

[2] F. E. Asimakopoulou, G. J. Tsekouras, I. F. Gonos, and I. A. Stathopulos, "Estimation of seasonal variation of ground resistance using artificial neural networks," *Electr. Power Syst. Res.*, vol. 94, pp. 113–121, Jan. 2013.

[3] C. Yu, Z. Fu, G. Wu, L. Zhou, X. Zhu, and M. Bao, "Configuration detection of substation grounding grid using transient electromagnetic method," *IEEE Trans. Ind. Electron.*, vol. 64, no. 8, pp. 6475–6483, Aug. 2017.

[4] J. He, R. Zeng, and B. Zhang, *Methodology and Technology for Power System Grounding*. Singapore: Wiley, 2013.

[5] Q. Li, S. Li, H. Zhao, X. Song, J. Qiu, C. Xue, W. Li, E. Hu, and S. Zhai, "Research on the influence of stray current on grounding grid and corresponding protection," in *Proc. IEEE 4th Conf. Energy Internet Energy Syst. Integr. (EI2)*, Oct. 2020, pp. 3631–3635.

[6] M. Chen, S. Liu, N. Zhao, H. Fu, and Y. Lv, "Fault diagnosis and location of electrified railway grounding grids based on intelligent algorithm," *Int. Trans. Electr. Energy Syst.*, vol. 31, no. 2, Feb. 2021, Art. no. e12719.

[7] C. Zhang, Y. Liao, X. Gao, J. Zhao, Y. Yuan, and R. Liao, "Research advances of soil corrosion of grounding grids," *Micromachines*, vol. 12, no. 5, p. 513, May 2021.

[8] X. Wang, Z. Fu, Y. Wang, R. Liu, and L. Chen, "A non-destructive testing method for fault detection of substation grounding grids," *Sensors*, vol. 19, no. 9, p. 2046, May 2019.

[9] Z. Fu, X. Wang, Q. Wang, X. Xu, N. Fu, and S. Qin, "Advances and challenges of corrosion and topology detection of grounding grid," *Appl. Sci.*, vol. 9, no. 11, p. 2290, Jun. 2019.

[10] S. Qin, Y. Wang, Z. Xu, X. Liao, L. Liu, and Z. Fu, "Fast resistivity imaging of transient electromagnetic using ANN," *IEEE Geosci. Remote Sens. Lett.*, vol. 16, no. 9, pp. 1373–1377, Sep. 2019.

[11] C. Yu, Z. Fu, Q. Wang, H.-M. Tai, and S. Qin, "A novel method for fault diagnosis of grounding grids," *IEEE Trans. Ind. Appl.*, vol. 51, no. 6, pp. 5182–5188, Nov./Dec. 2015.

[12] D. G. Koliushko and S. S. Rudenko, "Analysis of methods for monitoring of existing energy objects grounding devices state at the present stage," *Electr. Eng. Electromech.*, vol. 1, pp. 67–72, Feb. 2019.

[13] X.-L. Zhang, X.-H. Zhao, Y.-G. Wang, and N. Mo, "Development of an electrochemical *in situ* detection sensor for grounding grid corrosion," *Corrosion*, vol. 66, no. 7, Jul. 2010, Art. no. 076001.

[14] Y. Shao, M. Mu, B. Zhang, K. Nie, and Q. Liao, "Corrosion behavior of copper-clad steel bars with unclad two-end faces for grounding grids in the red clay soil," *J. Mater. Eng. Perform.*, vol. 26, no. 4, pp. 1751–1757, Apr. 2017.

[15] J. Li, H. Su, F. Chai, D.-M. Xue, L. Li, X.-Y. Li, and H.-M. Meng, "Corrosion behavior of low-carbon Cr micro-alloyed steel for grounding grids in simulated acidic soil," *J. Iron Steel Res. Int.*, vol. 25, no. 7, pp. 755–766, Jul. 2018.

[16] C. Yu, Z. Fu, X. Hou, H.-M. Tai, and X. Su, "Break-point diagnosis of grounding grids using transient electromagnetic apparent resistivity imaging," *IEEE Trans. Power Del.*, vol. 30, no. 6, pp. 2485–2491, Dec. 2015.

[17] K. Liu, F. Yang, X. Wang, B. Gao, X. Kou, M. Dong, and A. Jadoon, "A novel resistance network node potential measurement method and application in grounding grids corrosion diagnosis," *Prog. Electromagn. Res. M*, vol. 52, pp. 9–20, 2016.

[18] F. Yang, Y. Wang, M. Dong, X. Kou, D. Yao, X. Li, B. Gao, and I. Ullah, "A cycle voltage measurement method and application in grounding grids fault location," *Energies*, vol. 10, no. 11, p. 1929, Nov. 2017.

[19] M. Dong, Z. Shi, X. Li, G. Shao, F. Yang, D. Yao, and K. Zhang, "A diagnosis of grounding grid corrosion defects based on branch voltage disturbance," *IEEE Access*, vol. 8, pp. 36749–36756, 2020.

[20] Y. Zhang, B. Guo, X. He, C. Zhang, S. Li, and P. Li, "Design of multi-channel corrosion detection system for grounding grid in substation," *Univ. Politeh. Buchar. Sci. Bull. Ser. C Electr. Eng. Comput. Sci*, vol. 82, no. 2, pp. 265–278, 2020.

[21] A. Qamar, N. Shah, Z. Kaleem, Z. Uddin, and F. A. Orakzai, "Breakpoint diagnosis of substation grounding grid using derivative method," *Progr. Electromagn. Res. M*, vol. 57, pp. 73–80, 2017.

[22] A. Qamar, Z. Uddin, and F. Yang, "Inverse features extraction for substation grounding grid: Derivative and ICA combinatorial approach," *IET Gener., Transmiss. Distrib.*, vol. 13, no. 24, pp. 5457–5466, Dec. 2019.

[23] L. Kai, Y. Fan, Z. Songyang, Z. Liwei, H. Jiayuan, W. Xiaoyu, and I. Ullah, "Research on grounding grids imaging reconstruction based on magnetic detection electrical impedance tomography," *IEEE Trans. Magn.*, vol. 54, no. 3, pp. 1–4, Mar. 2018.

[24] A. Qamar, F. Yang, W. He, A. Jadoon, M. Z. Khan, and N. Xu, "Topology measurement of substation's grounding grid by using electromagnetic and derivative method," *Prog. Electromagn. Res. B*, vol. 67, pp. 71–90, 2016.

[25] Z. Fu, S. Song, X. Wang, J. Li, and H.-M. Tai, "Imaging the topology of grounding grids based on wavelet edge detection," *IEEE Trans. Magn.*, vol. 54, no. 4, pp. 1–8, Apr. 2018.

[26] A. Hannigan, "Effects of electric and magnetic fields on transmission line design, vol. 17, no. 4, July," Elect. Energy T&D Magazine Jaguar Expo, Brossard, QC, Canada, Tech. Rep., 2013. [Online]. Available: http://www.electricalenergyonline.com

AAMIR QAMAR received the Ph.D. degree in electrical engineering from Chongqing University, China, in 2016. During his Ph.D., he was with the State and Key Laboratory of Power Transmission and System Security and New Technology, Chongqing University. He is currently working as an Assistant Professor with COMSATS University Islamabad, Wah Campus. He is also working on the performance analysis of substation grounding grid and the fault localization of underground cables. His research interests include signal processing and electromagnetic.

SHAHID IQBAL received the bachelor's degree in electrical engineering from the University of Wah, Pakistan, in 2018, and the master's degree in electrical engineering from COMSATS University Islamabad, in 2020. His research interests include configuration detection and fault localization of the substation grounding grids.

SADIQ AHMAD (Member, IEEE) received the B.Sc. degree in electrical engineering from the University of Engineering and Technology, Peshawar, Pakistan, in 2009, and the M.S. and Ph.D. degrees in power engineering from COMSATS University Islamabad, Wah Cantt., Pakistan, in 2014 and 2020, respectively. He is currently working as a Lecturer with the Department of Electrical Engineering, COMSATS University Islamabad. His research interests include privacy preservation in smart meters, blockchain in smartgrids, security and privacy issues in smartgrids, cognitive radio networks, energy efficiency, green energy generation, resource optimization in power system engineering, control and optimization of microgrids/smartgrids, and optimization issues in power systems and smartgrids. He served in the Water and Power Development Authority (WAPDA), Pakistan, for one year and then joined Etisalat Telecommunication Company, where he served until April 2012. He won the Best Research Paper Award (2015) under the patronage of the Higher Education Commission, Government of Pakistan. He is a Reviewer of renowned international journals, such as IEEE Access, IEEE Transactions on Biomedical Engineering, *Applied Energy*, *Energies*, *International Transaction on Electrical Energy System* (Wiley), *Journal of Network and Computer Applications*, *Computers & Electrical Engineering*, and *Energy & Building*.

ABBAS Z. KOUZANI (Member, IEEE) received the B.Sc. degree in computer engineering from Sharif University of Technology, Iran, the M.Eng.Sc. degree in electrical and electronic engineering from The University of Adelaide, Australia, and the Ph.D. degree in electrical and electronic engineering from Flinders University, Australia. He was a Lecturer with the School of Engineering, Deakin University, Australia, and then a Senior Lecturer with the School of Electrical Engineering and Computer Science, University of Newcastle, Australia. He is currently a Professor with the School of Engineering, Deakin University. He provides research leadership in embedded, connected, and low-power devices, circuits, and instruments that incorporate sensing, actuation, control, wireless transmission, networking, and the IoT, data acquisition/storage/analysis, AI, energy harvesting, power management, and fabrication for tackling research questions relating to a variety of disciplines including healthcare, ecology, mining, infrastructure, automotive, manufacturing, energy, utilities, and agriculture. He has produced over 370 publications, including one book, 17 book chapters, 180 journal articles, and 181 fully refereed conference papers. He has three patents and two pending patents. He has been involved in over $15 million research grants, and has managed projects and delivered research solutions to over 25 Australian and International companies. He received several awards, including the Outstanding Contribution to Scholarly Publication Award from the School of Engineering, Deakin University, in 2019. He has supervised 24 research fellows/assistants and produced 28 Ph.D. and six master's students through research completions. He is also involved in the supervision of 12 Ph.D. students. He is the Director of Deakin University's Advanced Integrated Microsystems (AIM) Research Group.

M. A. PARVEZ MAHMUD (Member, IEEE) received the B.Sc. degree in electrical and electronic engineering and the M.Eng. degree in mechatronics engineering. After the successful completion of his Ph.D. degree in engineering with several awards, including the "Macquarie University Highly Commended Excellence in Higher Degree Research Award 2019," he worked as a Postdoctoral Research Associate and Academic with the School of Engineering, Macquarie University, Sydney. Besides, before coming to Australia, he worked as a Lecturer in mechatronics engineering with the World University of Bangladesh for more than two years and performed as a Researcher with Korea Institute of Machinery and Materials for about three years. He is currently supervising eight Ph.D. students in renewable energy, electric vehicles, advanced soft energy materials, energy sustainability, microgrid energy trading, machine learning, and artificial intelligence (AI). He is also an Alfred Deakin Postdoctoral Fellow of the School of Engineering, Deakin University, Melbourne, VIC, Australia. He has made significant research contributions in the area of energy sustainability, energy harvesting, artificial intelligence, and smart sensing, and published more than 120 scholarly articles, including two authored books, nine book chapters, 74 peer-reviewed journal articles, and 39 fully refereed conference proceedings (Google Scholar). His one more full book proposal has already been accepted by Elsevier to be published in 2021. His research interests include energy materials, energy harvesting, smart sensing, and energy sustainability.